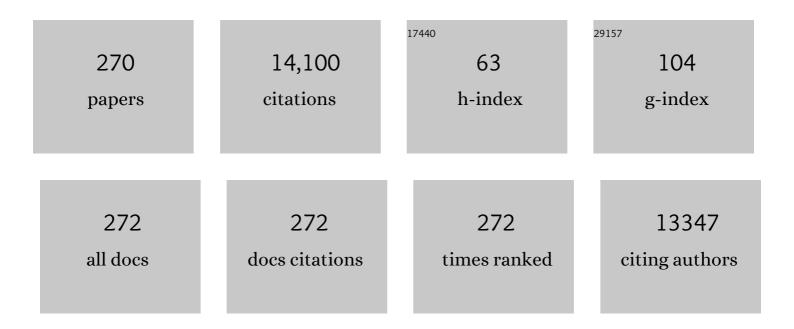
## Jianshe Lian

List of Publications by Year in descending order

Source: https://exaly.com/author-pdf/7874149/publications.pdf Version: 2024-02-01



#	Article	IF	CITATIONS
1	Ultra-strong and thermally stable nanocrystalline CrCoNi alloy. Journal of Materials Science and Technology, 2022, 106, 1-9.	10.7	21
2	Superhydrophobic brass surfaces with tunable water adhesion fabricated by laser texturing followed by heat treatment and their anti-corrosion ability. Applied Surface Science, 2022, 575, 151596.	6.1	34
3	Improving the corrosion resistance and biocompatibility of magnesium alloy via composite coatings of calcium phosphate/carbonate induced by silane. Progress in Organic Coatings, 2022, 163, 106653.	3.9	12
4	A polydopamine-based calcium phosphate/graphene oxide composite coating on magnesium alloy to improve corrosion resistance and biocompatibility for biomedical applications. Materialia, 2022, 21, 101315.	2.7	19
5	Effect of Al Addition on the Microstructure and Mechanical Properties of Al <sub>x</sub> CrCoNi Medium Entropy Alloys Prepared via the Magnetron Coâ€ <del>S</del> puttering. Advanced Engineering Materials, 2022, 24, .	3.5	4
6	Effects of cold-rolling and subsequent annealing on the nano-mechanical and creep behaviors of CrCoNi medium-entropy alloy. Materials Science & Engineering A: Structural Materials: Properties, Microstructure and Processing, 2022, 839, 142802.	5.6	10
7	Corrosion Resistance and Biocompatibility of Calcium Phosphate Coatings with a Micro–Nanofibrous Porous Structure on Biodegradable Magnesium Alloys. ACS Applied Bio Materials, 2022, 5, 1528-1537.	4.6	13
8	Boosting the OER/ORR/HER activity of Ru-doped Ni/Co oxides heterostructure. Chemical Engineering Journal, 2022, 439, 135634.	12.7	49
9	<i>In situ</i> phosphating of Zn-doped bimetallic skeletons as a versatile electrocatalyst for water splitting. Energy and Environmental Science, 2022, 15, 2425-2434.	30.8	50
10	Uniting tensile ductility with ultrahigh strength via composition undulation. Nature, 2022, 604, 273-279.	27.8	80
11	Unveiling the grain boundary-related effects on the incipient plasticity and dislocation behavior in nanocrystalline CrCoNi medium-entropy alloy. Journal of Materials Science and Technology, 2022, 127, 98-107.	10.7	9
12	Improvement of corrosion resistance of H59 brass through fabricating superhydrophobic surface using laser ablation and heating treatment. Corrosion Science, 2021, 180, 109186.	6.6	54
13	Cu-doped Ni3S2 nanosheet arrays on Ni foam as an efficient electrocatalyst for oxygen evolution reaction. Journal of Solid State Chemistry, 2021, 293, 121776.	2.9	14
14	MoS <sub>2</sub> Nanosheet-Polypyrrole Composites Deposited on Reduced Graphene Oxide for Supercapacitor Applications. ACS Applied Nano Materials, 2021, 4, 1330-1339.	5.0	47
15	Grain size dependent microstructure and texture evolution during dynamic deformation of nanocrystalline face-centered cubic materials. Acta Materialia, 2021, 216, 117088.	7.9	10
16	P- N heterojunction NiO/ZnO electrode with high electrochemical performance for supercapacitor applications. Electrochimica Acta, 2021, 392, 138976.	5.2	23
17	The microstructure, mechanical properties, corrosion performance and biocompatibility of hydroxyapatite reinforced ZK61 magnesium-matrix biological composite. Journal of the Mechanical Behavior of Biomedical Materials, 2021, 123, 104759.	3.1	15
18	Interface Engineering of CoP <sub>3</sub> /Ni <sub>2</sub> P for Boosting the Wide pH Range Water-Splitting Activity. ACS Applied Materials & Interfaces, 2021, 13, 52598-52609.	8.0	20

#	Article	IF	CITATIONS
19	Enhanced corrosion resistance and biocompatibility of polydopamine/dicalcium phosphate dihydrate/collagen composite coating on magnesium alloy for orthopedic applications. Journal of Alloys and Compounds, 2020, 817, 152782.	5.5	37
20	Facile synthesis clusters of sheet-like Ni3S4/CuS nanohybrids with ultrahigh supercapacitor performance. Journal of Solid State Chemistry, 2020, 282, 121088.	2.9	21
21	Enhancing the brightness and saturation of noniridescent structural colors by optimizing the grain size. Nanoscale Advances, 2020, 2, 4581-4590.	4.6	5
22	Reduced core-shell structured MnCo2O4@MnO2 nanosheet arrays with oxygen vacancies grown on Ni foam for enhanced-performance supercapacitors. Journal of Alloys and Compounds, 2020, 846, 156504.	5.5	48
23	Improvements of Corrosion Resistance and Antibacterial Properties of Hydroxyapatite/Cupric Oxide Doped Titania Composite Coatings on Degradable Magnesium Alloys. Langmuir, 2020, 36, 13937-13948.	3.5	19
24	Enhanced corrosion resistance and biocompatibility of biodegradable magnesium alloy modified by calcium phosphate/collagen coating. Surface and Coatings Technology, 2020, 401, 126318.	4.8	59
25	Comparison of corrosion resistance and biocompatibility of magnesium phosphate (MgP), zinc phosphate (ZnP) and calcium phosphate (CaP) conversion coatings on Mg alloy. Surface and Coatings Technology, 2020, 397, 125919.	4.8	57
26	A multifunctional polypyrrole/zinc oxide composite coating on biodegradable magnesium alloys for orthopedic implants. Colloids and Surfaces B: Biointerfaces, 2020, 194, 111186.	5.0	38
27	Nanostructuring as a route to achieve ultra-strong high- and medium-entropy alloys with high creep resistance. Journal of Alloys and Compounds, 2020, 830, 154656.	5.5	21
28	Thermodynamic analysis on wetting states and wetting state transitions of rough surfaces. Advances in Colloid and Interface Science, 2020, 278, 102136.	14.7	31
29	Threeâ€Dimensional ZnMn <sub>2</sub> O <sub>4</sub> Nanoparticles/Carbon Cloth Anodes for Highâ€Performance Flexible Lithiumâ€Ion Batteries. ChemistrySelect, 2020, 5, 2372-2378.	1.5	9
30	Effect of pH value and preparation temperature on the formation of magnesium phosphate conversion coatings on AZ31 magnesium alloy. Applied Surface Science, 2019, 492, 314-327.	6.1	74
31	Facile synthesis of copper selenide with fluffy intersected-nanosheets decorating nanotubes structure for efficient oxygen evolution reaction. International Journal of Hydrogen Energy, 2019, 44, 22983-22990.	7.1	21
32	Reversible wettability transition between superhydrophilicity and superhydrophobicity through alternate heating-reheating cycle on laser-ablated brass surface. Applied Surface Science, 2019, 492, 349-361.	6.1	52
33	Nanoindentation creep deformation behaviour of high nitrogen nickel-free austenitic stainless steel. Materials Science and Technology, 2019, 35, 1592-1599.	1.6	6
34	Hierarchical Cu(OH)2/Co2(OH)2CO3 nanohybrid arrays grown on copper foam for high-performance battery-type supercapacitors. Journal of Materials Science: Materials in Electronics, 2019, 30, 11952-11963.	2.2	16
35	Charge Storage by Electrochemical Reaction of Water Bilayers Absorbed on MoS2 Monolayers. Scientific Reports, 2019, 9, 3980.	3.3	16
36	Nanoindentation creep behavior and its relation to activation volume and strain rate sensitivity of nanocrystalline Cu. Materials Science & Engineering A: Structural Materials: Properties, Microstructure and Processing, 2019, 751, 35-41.	5.6	30

#	Article	IF	CITATIONS
37	Invigorating the catalytic performance of CoP through interfacial engineering by Ni <sub>2</sub> P precipitation. Journal of Materials Chemistry A, 2019, 7, 26177-26186.	10.3	13
38	Rational fabrication of nanosheet-dewy NiMoO4/Ni3S2 nanohybrid for efficient hybrid supercapacitor. Journal of Alloys and Compounds, 2019, 783, 399-408.	5.5	21
39	Improving the Degradation Resistance and Surface Biomineralization Ability of Calcium Phosphate Coatings on a Biodegradable Magnesium Alloy via a Sol-Gel Spin Coating Method. Journal of the Electrochemical Society, 2018, 165, C155-C161.	2.9	26
40	Dual Superlyophobic Copper Foam with Good Durability and Recyclability for High Flux, High Efficiency, and Continuous Oil–Water Separation. ACS Applied Materials & Interfaces, 2018, 10, 9841-9848.	8.0	92
41	CuS/MnS composite hexagonal nanosheet clusters: Synthesis and enhanced pseudocapacitive properties. Electrochimica Acta, 2018, 271, 425-432.	5.2	49
42	Strain rate dependence of tensile strength and ductility of nano and ultrafine grained coppers. Materials Science & Engineering A: Structural Materials: Properties, Microstructure and Processing, 2018, 712, 341-349.	5.6	16
43	Hydroxyapatite/Titania Composite Coatings on Biodegradable Magnesium Alloy for Enhanced Corrosion Resistance, Cytocompatibility and Antibacterial Properties. Journal of the Electrochemical Society, 2018, 165, C962-C972.	2.9	38
44	Ni Foamâ€Ni <sub>3</sub> S <sub>2</sub> @Ni(OH) <sub>2</sub> â€Graphene Sandwich Structure Electrode Materials: Facile Synthesis and High Supercapacitor Performance. Chemistry - A European Journal, 2017, 23, 4128-4136.	3.3	43
45	Arrays of hierarchical nickel sulfides/MoS2 nanosheets supported on carbon nanotubes backbone as advanced anode materials for asymmetric supercapacitor. Journal of Power Sources, 2017, 343, 373-382.	7.8	162
46	A Strategy for Synthesis of Nanosheets Consisting of Alternating Spinel Li <sub>4</sub> Ti <sub>5</sub> O <sub>12</sub> and Rutile TiO <sub>2</sub> Lamellas for High-Rate Anodes of Lithium-Ion Batteries. ACS Applied Materials & Interfaces, 2017, 9, 4649-4657.	8.0	42
47	Reduced graphene oxide wrapped Fe3O4–Co3O4 yolk–shell nanostructures for advanced catalytic oxidation based on sulfate radicals. Applied Surface Science, 2017, 396, 945-954.	6.1	47
48	Facile Synthesis ZnS/ZnO/Ni(OH)2 Composites Grown on Ni Foam: A Bifunctional Materials for Photocatalysts and Supercapacitors. Scientific Reports, 2017, 7, 3021.	3.3	40
49	Plastic deformation and fracture behaviour of high-nitrogen nickel-free austenitic stainless steel. Materials Science and Technology, 2017, 33, 1635-1644.	1.6	9
50	Mapping the strain-rate and grain-size dependence of deformation behaviors in nanocrystalline face-centered-cubic Ni and Ni-based alloys. Journal of Alloys and Compounds, 2017, 709, 566-574.	5.5	25
51	How to improve the stability and rate performance of lithium-ion batteries with transition metal oxide anodes. Journal of Materials Research, 2017, 32, 16-36.	2.6	36
52	Reusable Co <sub>x</sub> Ni <sub>1â^'x</sub> dye adsorbents as supercapacitor electrode materials. Journal of Materials Chemistry A, 2017, 5, 8095-8107.	10.3	13
53	Fabrication of Superhydrophobic Calcium Phosphate Coating on Mg-Zn-Ca alloy and Its Corrosion Resistance. Journal of Materials Engineering and Performance, 2017, 26, 6117-6129.	2.5	19
54	High Density Arrayed Ni/NiO Core-shell Nanospheres Evenly Distributed on Graphene for Ultrahigh Performance Supercapacitor. Scientific Reports, 2017, 7, 17709.	3.3	64

#	Article	IF	CITATIONS
55	Synthesis of polygonal Co <sub>3</sub> Sn <sub>2</sub> nanostructure with enhanced magnetic properties. RSC Advances, 2016, 6, 39818-39822.	3.6	13
56	One-pot hydrothermal synthesis of octahedral CoFe/CoFe <sub>2</sub> O <sub>4</sub> submicron composite as heterogeneous catalysts with enhanced peroxymonosulfate activity. Journal of Materials Chemistry A, 2016, 4, 9455-9465.	10.3	128
57	Improvement of the Biodegradation Property and Biomineralization Ability of Magnesium–Hydroxyapatite Composites with Dicalcium Phosphate Dihydrate and Hydroxyapatite Coatings. ACS Biomaterials Science and Engineering, 2016, 2, 818-828.	5.2	66
58	Composite Microstructure and Formation Mechanism of Calcium Phosphate Conversion Coating on Magnesium Alloy. Journal of the Electrochemical Society, 2016, 163, G138-G143.	2.9	30
59	Preparation and corrosion behaviors of calcium phosphate conversion coating on magnesium alloy. Surface and Coatings Technology, 2016, 307, 99-108.	4.8	85
60	A Ni <sub>1â^'x</sub> Zn <sub>x</sub> S/Ni foam composite electrode with multi-layers: one-step synthesis and high supercapacitor performance. Journal of Materials Chemistry A, 2016, 4, 12929-12939.	10.3	52
61	A novel open architecture built by ultra-fine single-crystal Co <sub>2</sub> (CO <sub>3</sub> )(OH) <sub>2</sub> nanowires and reduced graphene oxide for asymmetric supercapacitors. Journal of Materials Chemistry A, 2016, 4, 17171-17179.	10.3	74
62	Growth of vertically aligned Co <sub>3</sub> S <sub>4</sub> /CoMo <sub>2</sub> S <sub>4</sub> ultrathin nanosheets on reduced graphene oxide as a high-performance supercapacitor electrode. Journal of Materials Chemistry A, 2016, 4, 18857-18867.	10.3	150
63	Robust superhydrophobic surface on Al substrate with durability, corrosion resistance and ice-phobicity. Scientific Reports, 2016, 6, 20933.	3.3	79
64	High Efficient Photo-Fenton Catalyst of α-Fe2O3/MoS2 Hierarchical Nanoheterostructures: Reutilization for Supercapacitors. Scientific Reports, 2016, 6, 31591.	3.3	68
65	A unique porous architecture built by ultrathin wrinkled NiCoO <sub>2</sub> /rGO/NiCoO <sub>2</sub> sandwich nanosheets for pseudocapacitance and Li ion storage. Journal of Materials Chemistry A, 2016, 4, 10304-10313.	10.3	72
66	One-step synthesis of Ni3Sn2@reduced graphene oxide composite with enhanced electrochemical lithium storage properties. Electrochimica Acta, 2016, 192, 188-195.	5.2	39
67	Plastic deformation behavior during unloading in compressive cyclic test of nanocrystalline copper. Materials Science & Engineering A: Structural Materials: Properties, Microstructure and Processing, 2016, 651, 999-1009.	5.6	26
68	Plastic flow behavior and its relationship to tensile mechanical properties of high nitrogen nickel-free austenitic stainless steel. Materials Science & Engineering A: Structural Materials: Properties, Microstructure and Processing, 2016, 662, 432-442.	5.6	25
69	Nanostructured Co <sub>x</sub> Ni <sub>1â^'x</sub> bimetallic alloys for high efficient and ultrafast adsorption: experiments and first-principles calculations. RSC Advances, 2016, 6, 9209-9220.	3.6	12
70	In situ prepared reduced graphene oxide/CoO nanowires mutually-supporting porous structure with enhanced lithium storage performance. Electrochimica Acta, 2016, 190, 276-284.	5.2	58
71	Carbon-Encapsulated Co3O4 Nanoparticles as Anode Materials with Super Lithium Storage Performance. Scientific Reports, 2015, 5, 16629.	3.3	73
72	Ultrathin Mesoporous NiCo <sub>2</sub> O <sub>4</sub> Nanosheet Networks as Highâ€Performance Anodes for Lithium Storage. ChemPlusChem, 2015, 80, 1725-1731.	2.8	31

#	Article	IF	CITATIONS
73	Electromagnetic shielding and corrosion resistance of electroless Ni-P and Ni-P-Cu coatings on polymer/carbon fiber composites. Polymer Composites, 2015, 36, 923-930.	4.6	32
74	A novel interfacial synthesis of MnO–NiO–reduced graphene oxide hybrid with enhanced pseudocapacitance performance. RSC Advances, 2015, 5, 54138-54147.	3.6	3
75	Dry sliding wear behavior of extruded Mg-Sn-Yb alloy. Journal of Rare Earths, 2015, 33, 77-85.	4.8	20
76	Preparation and photocatalytic performance of Cu-doped TiO2 nanoparticles. Transactions of Nonferrous Metals Society of China, 2015, 25, 504-509.	4.2	115
77	Glucose-assisted generation of assembled mesoporous ZnO sheets with highly efficient photocatalytic performance. Materials Science in Semiconductor Processing, 2015, 39, 680-685.	4.0	6
78	Effects of loading strain rate and stacking fault energy on nanoindentation creep behaviors of nanocrystalline Cu, Ni-20 wt.%Fe and Ni. Journal of Alloys and Compounds, 2015, 647, 670-680.	5.5	55
79	Enhancing the corrosion resistance and surface bioactivity of a calcium-phosphate coating on a biodegradable AZ60 magnesium alloy via a simple fluorine post-treatment method. RSC Advances, 2015, 5, 56001-56010.	3.6	41
80	One-step synthesis of nanostructured Bi–Bi <sub>2</sub> O <sub>2</sub> CO <sub>3</sub> –ZnO composites with enhanced photocatalytic performance. CrystEngComm, 2015, 17, 3809-3819.	2.6	20
81	Ni–Zn binary system hydroxide, oxide and sulfide materials: synthesis and high supercapacitor performance. Journal of Materials Chemistry A, 2015, 3, 23333-23344.	10.3	107
82	Single-crystalline Ni(OH)2nanosheets vertically aligned on a three-dimensional nanoporous metal for high-performance asymmetric supercapacitors. Journal of Materials Chemistry A, 2015, 3, 23412-23419.	10.3	45
83	Deformation behavior of an extruded Mg–Dy–Zn alloy with long period stacking ordered phase. Materials Science & Engineering A: Structural Materials: Properties, Microstructure and Processing, 2015, 622, 52-60.	5.6	16
84	Understanding the microscopic deformation mechanism and macroscopic mechanical behavior of nanocrystalline Ni by the long-term stress relaxation test. International Journal of Modern Physics B, 2014, 28, 1450124.	2.0	5
85	The Synthesis and Electrochemical Behavior of High-Nitrogen Nickel-Free Austenitic Stainless Steel. Journal of Materials Engineering and Performance, 2014, 23, 3957-3962.	2.5	16
86	High resolution transmission electron microscopic in-situ observations of plastic deformation of compressed nanocrystalline gold. Journal of Applied Physics, 2014, 116, 103518.	2.5	3
87	Dislocation Evolution in Nanograins during Successive Stress Relaxation. Advanced Engineering Materials, 2014, 16, 413-420.	3.5	1
88	Synthesis of amorphous TiO2 modified ZnO nanorod film with enhanced photocatalytic properties. Applied Surface Science, 2014, 299, 97-104.	6.1	53
89	Toward Tandem Photovoltaic Devices Employing Nanoarray Graphene-Based Sheets. Journal of Physical Chemistry C, 2014, 118, 2385-2390.	3.1	6
90	Impact dynamics of water droplets on Cu films with three-level hierarchical structures. Journal of Materials Science, 2014, 49, 3379-3390.	3.7	14

#	Article	IF	CITATIONS
91	Enhanced Photocatalytic Performance of Supported Fe Doped ZnO Nanorod Arrays Prepared by Wet Chemical Method. Catalysis Letters, 2014, 144, 347-354.	2.6	26
92	Bandgap variation in grain size controlled nanostructured CdO thin films deposited by pulsed-laser method. Journal of Materials Science: Materials in Electronics, 2014, 25, 1003-1012.	2.2	23
93	Role of Edge Geometry and Magnetic Interaction in Opening Bandgap of Lowâ€Dimensional Graphene. ChemPhysChem, 2014, 15, 958-965.	2.1	6
94	Markedly enhanced coercive field and Congo red adsorption capability of cobalt ferrite induced by the doping of non-magnetic metal ions. Chemical Engineering Journal, 2014, 241, 384-392.	12.7	35
95	Effect of cold rolling on tensile properties and microstructure of high nitrogen alloyed austenitic steel. Materials Science and Technology, 2014, 30, 146-151.	1.6	20
96	Cu surfaces with controlled structures: From intrinsically hydrophilic to apparently superhydrophobic. Applied Surface Science, 2014, 290, 320-326.	6.1	28
97	Characterizing deformed ultrafine-grained and nanocrystalline materials using transmission Kikuchi diffraction in a scanning electron microscope. Acta Materialia, 2014, 62, 69-80.	7.9	142
98	Solvothermal synthesis of nanocrystalline ZnO with excellent photocatalytic performance. Journal of Materials Science: Materials in Electronics, 2014, 25, 5518-5523.	2.2	8
99	Ca-P conversion coating on AZ60 magnesium alloy for biomedical application. Chemical Research in Chinese Universities, 2014, 30, 543-548.	2.6	4
100	CaGdAlO <sub>4</sub> :Tb <sup>3+</sup> /Eu <sup>3+</sup> as promising phosphors for full-color field emission displays. Journal of Materials Chemistry C, 2014, 2, 9924-9933.	5.5	107
101	Biocompatible DCPD Coating Formed on AZ91D Magnesium Alloy by Chemical Deposition and Its Corrosion Behaviors in SBF. Journal of Bionic Engineering, 2014, 11, 610-619.	5.0	27
102	Nanostructured Mn <sub>3</sub> O <sub>4</sub> –reduced graphene oxide hybrid and its applications for efficient catalytic decomposition of Orange II and high lithium storage capacity. RSC Advances, 2014, 4, 41838-41847.	3.6	40
103	Structural, optical and electrical characterization of gadolinium and indium doped cadmium oxide/p-silicon heterojunctions for solar cell applications. RSC Advances, 2014, 4, 52451-52460.	3.6	33
104	Enhancing photocatalytic activity of disorder-engineered C/TiO <sub>2</sub> and TiO <sub>2</sub> nanoparticles. Journal of Materials Chemistry A, 2014, 2, 7439-7445.	10.3	130
105	Effect of strain rate on tensile properties of electric brush-plated nanocrystalline copper. Materials Science & Engineering A: Structural Materials: Properties, Microstructure and Processing, 2014, 618, 621-628.	5.6	22
106	New insight into modulated up-conversion luminescent silica nanotubes as efficient adsorbents for colored effluents. Dalton Transactions, 2014, 43, 15457-15464.	3.3	9
107	Disordered ZnO nanoparticles with extremely intense deep-level emission and enhanced photocatalytic activity. Applied Surface Science, 2014, 313, 888-895.	6.1	12
108	Synthesis of a Thin-Layer MnO <sub>2</sub> Nanosheet-Coated Fe <sub>3</sub> O <sub>4</sub> Nanocomposite as a Magnetically Separable Photocatalyst. Langmuir, 2014, 30, 7006-7013.	3.5	126

#	Article	IF	CITATIONS
109	Enhanced optical absorption and photocatalytic activity of Cu/N-codoped TiO2 nanocrystals. Materials Science in Semiconductor Processing, 2014, 24, 247-253.	4.0	28
110	Superhydrophilic Cu-doped TiO2 thin film for solar-driven photocatalysis. Ceramics International, 2014, 40, 5107-5110.	4.8	55
111	Revealing the intrinsic dislocation storage capability in nanocrystalline nickel. Materials Letters, 2014, 127, 20-23.	2.6	2
112	Optical properties and photocatalytic activity of Nd-doped ZnO powders. Transactions of Nonferrous Metals Society of China, 2014, 24, 1434-1439.	4.2	51
113	Microstructures and mechanical properties of extruded Mg–2Sn–xYb (x=0, 0.1, 0.5Âat.%) sheets. Journal of Magnesium and Alloys, 2014, 2, 257-264.	11.9	10
114	Preparation and Corrosion Behavior of Calcium Phosphate and Hydroxyapatite Conversion Coatings on AM60 Magnesium Alloy. Journal of the Electrochemical Society, 2013, 160, C536-C541.	2.9	46
115	Stable ductility of an electrodeposited nanocrystalline Ni–20wt.%Fe alloy in tensile plastic deformation. Journal of Alloys and Compounds, 2013, 553, 99-105.	5.5	9
116	Structure and photocatalytic property of Mo-doped TiO2 nanoparticles. Powder Technology, 2013, 244, 9-15.	4.2	118
117	High resolution transmission electron microscopy in situ investigation into the spontaneous coalescence of gold nanoparticles at room temperature. RSC Advances, 2013, 3, 24017.	3.6	5
118	Nanocrystalline ZnO films prepared by pulsed laser deposition and their abnormal optical properties. Applied Surface Science, 2013, 283, 781-787.	6.1	24
119	Multifunctional NaYF4:Yb/Er/Gd nanocrystal decorated SiO2 nanotubes for anti-cancer drug delivery and dual modal imaging. RSC Advances, 2013, 3, 8517.	3.6	18
120	Stability of indium–tin-oxide and its optical properties: A first-principles study. Journal of Physics and Chemistry of Solids, 2013, 74, 446-451.	4.0	8
121	Synthesis and photoluminescence of Y and Cd co-doped ZnO nanopowder. Transactions of Nonferrous Metals Society of China, 2013, 23, 2336-2340.	4.2	13
122	Electroless nickel, alloy, composite and nano coatings – A critical review. Journal of Alloys and Compounds, 2013, 571, 183-204.	5.5	700
123	Structural, optical and electrical properties of cerium and gadolinium doped CdO thin films. Applied Surface Science, 2013, 274, 365-370.	6.1	60
124	Effects of passivation on the properties of Ni-P alloy coating deposited on CFs reinforced PEEK. Surface and Coatings Technology, 2013, 232, 269-274.	4.8	19
125	A new method to prepare MgO and base for further electroless nickel deposition on magnesium substrate. International Journal of Surface Science and Engineering, 2013, 7, 97.	0.4	3
126	Preparation of Nanocrystalline Cu Films by Brush-Plating. Integrated Ferroelectrics, 2012, 137, 52-60.	0.7	2

#	Article	IF	CITATIONS
127	INFLUENCE OF SURFACTANTS ON THE CORROSION PROPERTIES OF CHROMIUM-FREE ELECTROLESS NICKEL DEPOSIT ON MAGNESIUM ALLOY. Surface Review and Letters, 2012, 19, 1250025.	1.1	3
128	High-speed creep process mediated by rapid dislocation absorption in nanocrystalline Cu. Journal of Applied Physics, 2012, 111, 063506.	2.5	16
129	Structure and Photocatalysis of TiO <sub>2</sub> /ZnO Double-Layer Film Prepared by Pulsed Laser Deposition. Materials Transactions, 2012, 53, 463-468.	1.2	21
130	Superhydrophobic Behavior and Optical Properties of ZnO Film Fabricated by Hydrothermal Method. Journal of Materials Science and Technology, 2012, 28, 103-108.	10.7	12
131	Microstructure and Mechanical Properties of an Extruded Mg-2Dy-0.5Zn Alloy. Journal of Materials Science and Technology, 2012, 28, 543-551.	10.7	23
132	The performance of surfactant on the surface characteristics of electroless nickel coating on magnesium alloy. Progress in Organic Coatings, 2012, 74, 788-793.	3.9	63
133	Enhanced UV emission of Y-doped ZnO nanoparticles. Applied Surface Science, 2012, 258, 6735-6738.	6.1	76
134	Micro-twins TiO2 nanorods grown on seeded ZnO film. Journal of Crystal Growth, 2012, 344, 1-5.	1.5	4
135	Photocatalytic property of Fe doped anatase and rutile TiO2 nanocrystal particles prepared by sol–gel technique. Applied Surface Science, 2012, 263, 260-265.	6.1	95
136	Self-assembly of ultrathin porous NiO nanosheets/graphene hierarchical structure for high-capacity and high-rate lithium storage. Journal of Materials Chemistry, 2012, 22, 2844.	6.7	248
137	External Electric Field Catalyzed N <sub>2</sub> O Decomposition on Mn-Embedded Graphene. Journal of Physical Chemistry C, 2012, 116, 20342-20348.	3.1	44
138	Structural Selectivity of CO Oxidation on Fe/N/C Catalysts. Journal of Physical Chemistry C, 2012, 116, 17572-17579.	3.1	54
139	Potential dependent and structural selectivity of the oxygen reduction reaction on nitrogen-doped carbon nanotubes: a density functional theory study. Physical Chemistry Chemical Physics, 2012, 14, 11715.	2.8	52
140	Deformation-induced localized solid-state amorphization in nanocrystalline nickel. Scientific Reports, 2012, 2, 493.	3.3	53
141	Optical and magnetic properties of Ndâ€doped ZnO nanoparticles. Crystal Research and Technology, 2012, 47, 713-718.	1.3	61
142	Optical properties of Cu-doped ZnO nanoparticles experimental and first-principles theory research. Journal of Materials Science: Materials in Electronics, 2012, 23, 1521-1526.	2.2	22
143	Synthesis and optical properties of ZnO nanorods on indium tin oxide substrate. Applied Surface Science, 2011, 258, 93-97.	6.1	17
144	Double-peak ageing behavior of Mg–2Dy–0.5Zn alloy. Journal of Alloys and Compounds, 2011, 509, 8268-8275.	5.5	31

#	Article	IF	CITATIONS
145	High corrosion resistance of electroless Ni-P with chromium-free conversion pre-treatments on AZ91D magnesium alloy. Transactions of Nonferrous Metals Society of China, 2011, 21, 921-928.	4.2	32
146	Preparation of nano-silver iodide powders and their efficiency as ice-nucleating agent in weather modification. Advanced Powder Technology, 2011, 22, 613-616.	4.1	12
147	Effects of Process Parameters on Microstructure and Hardness of Layers by Laser Cladding. ISIJ International, 2011, 51, 441-447.	1.4	17
148	The deformation and fracture behavior of an electrodeposited nanocrystalline Ni under compression. Materials Science & Engineering A: Structural Materials: Properties, Microstructure and Processing, 2011, 528, 7878-7886.	5.6	8
149	Experimental and firstâ€principle investigation of Cuâ€doped ZnO ferromagnetic powders. Crystal Research and Technology, 2011, 46, 1143-1148.	1.3	22
150	Synthesis and optical properties of flower-like ZnO nanorods by thermal evaporation method. Applied Surface Science, 2011, 257, 5083-5087.	6.1	196
151	Structural, optical and electrical properties of Zn1â^xCdxO thin films prepared by PLD. Applied Surface Science, 2011, 257, 5657-5662.	6.1	45
152	An elevated temperature Mg–Dy–Zn alloy with long period stacking ordered phase by extrusion. Materials Science & Engineering A: Structural Materials: Properties, Microstructure and Processing, 2011, 528, 3609-3614.	5.6	54
153	Optical and electrical properties of Sn-doped CdO thin films obtained by pulse laser deposition. Vacuum, 2011, 85, 861-865.	3.5	100
154	Annealing effect on the photoluminescence properties of ZnO nanorod array prepared by a PLD-assistant wet chemical method. Materials Characterization, 2010, 61, 1239-1244.	4.4	62
155	Optical and electrical properties of In-doped CdO thin films fabricated by pulse laser deposition. Applied Surface Science, 2010, 256, 2910-2914.	6.1	80
156	The origin of the ultrahigh strength and good ductility in nanotwinned copper. Materials Science & Engineering A: Structural Materials: Properties, Microstructure and Processing, 2010, 527, 4270-4274.	5.6	23
157	Microstructure and wear property of laser cladding Al+SiC powders on AZ91D magnesium alloy. Optics and Lasers in Engineering, 2010, 48, 526-532.	3.8	71
158	Dual-phase nanocrystalline Ni–Co alloy with high strength and enhanced ductility. Journal of Materials Research, 2010, 25, 401-405.	2.6	5
159	ENHANCED TENSILE DUCTILITY IN AN ELECTRODEPOSITED <font>CU</font> WITH NANO-SIZED GROWTH TWINS. International Journal of Modern Physics B, 2010, 24, 2537-2542.	2.0	3
160	IMPROVED MECHANICAL PROPERTY OF ELECTRODEPOSITED NANOCRYSTALLINE NICKEL-COBALT ALLOY. International Journal of Modern Physics B, 2010, 24, 2285-2290.	2.0	1
161	Tensile-relaxation behavior of electrodeposited nanocrystalline Ni. Journal of Applied Physics, 2010, 108, 054319.	2.5	11
162	Enhanced ductility of high-strength electrodeposited nanocrystalline Ni–Co alloy with fine grain size. Journal of Alloys and Compounds, 2010, 504, S439-S442.	5.5	25

#	Article	IF	CITATIONS
163	Effect of grain size on corrosion behavior of electrodeposited bulk nanocrystalline Ni. Transactions of Nonferrous Metals Society of China, 2010, 20, 82-89.	4.2	112
164	Organic-magnesium complex conversion coating on AZ91D magnesium alloy. Transactions of Nonferrous Metals Society of China, 2010, 20, s643-s647.	4.2	4
165	Compressive creep behavior of an electric brush-plated nanocrystalline Cu at room temperature. Journal of Applied Physics, 2009, 106, .	2.5	16
166	The grain refinement mechanism of electrodeposited copper. Journal of Materials Research, 2009, 24, 3226-3236.	2.6	6
167	Study of the formation and growth of tannic acid based conversion coating on AZ91D magnesium alloy. Surface and Coatings Technology, 2009, 204, 736-747.	4.8	87
168	Microstructure and properties of thin wall by laser cladding forming. Journal of Materials Processing Technology, 2009, 209, 4970-4976.	6.3	35
169	Controlling growth of ZnO rods by polyvinylpyrrolidone (PVP) and their optical properties. Applied Surface Science, 2009, 255, 6978-6984.	6.1	66
170	Surface Energy and Electronic Structures of Ag Quasicrystal Clusters. Journal of Physical Chemistry C, 2009, 113, 1168-1170.	3.1	36
171	Modeling of the Melting Point, Debye Temperature, Thermal Expansion Coefficient, and the Specific Heat of Nanostructured Materials. Journal of Physical Chemistry C, 2009, 113, 16896-16900.	3.1	139
172	Visible-light photocatalytic activity of nitrogen-doped TiO2 thin film prepared by pulsed laser deposition. Applied Surface Science, 2008, 254, 4620-4625.	6.1	84
173	A novel electrodeposited nanostructured Ni coating with grain size gradient distribution. Surface and Coatings Technology, 2008, 203, 142-147.	4.8	22
174	Visible-light photocatalysis in nitrogen–carbon-doped TiO2 films obtained by heating TiO2 gel–film in an ionized N2 gas. Thin Solid Films, 2008, 516, 1736-1742.	1.8	108
175	Electroless Ni-P deposition on magnesium alloy from a sulfate bath. Journal Wuhan University of Technology, Materials Science Edition, 2008, 23, 60-64.	1.0	4
176	The Optimal Grain Sized Nanocrystalline Ni with High Strength and Good Ductility Fabricated by a Direct Current Electrodeposition. Advanced Engineering Materials, 2008, 10, 539-546.	3.5	31
177	High strength and high ductility of electrodeposited nanocrystalline Ni with a broad grain size distribution. Materials Science & Engineering A: Structural Materials: Properties, Microstructure and Processing, 2008, 487, 410-416.	5.6	69
178	Electroless Ni-P/Ni-B duplex coatings for improving the hardness and the corrosion resistance of AZ91D magnesium alloy. Applied Surface Science, 2008, 254, 4949-4955.	6.1	94
179	Modeling size and surface effects on ZnS phase selection. Chemical Physics Letters, 2008, 455, 202-206.	2.6	29
180	Electroless Ni–Sn–P coating on AZ91D magnesium alloy and its corrosion resistance. Surface and Coatings Technology, 2008, 202, 2570-2576.	4.8	87

#	Article	IF	CITATIONS
181	Photocatalytic activity of TiO2 films with mixed anatase and rutile structures prepared by pulsed laser deposition. Thin Solid Films, 2008, 516, 3394-3398.	1.8	75
182	Effects of seed layer on the structure and property of zinc oxide thin films electrochemically deposited on ITO-coated glass. Applied Surface Science, 2008, 254, 6605-6610.	6.1	32
183	An organic chromium-free conversion coating on AZ91D magnesium alloy. Applied Surface Science, 2008, 255, 2322-2328.	6.1	68
184	Strain rate dependence of tensile ductility in an electrodeposited Cu with ultrafine grain size. Materials Science & Engineering A: Structural Materials: Properties, Microstructure and Processing, 2008, 479, 136-141.	5.6	28
185	Influence of preparation methods on photoluminescence properties of ZnO films on quartz glass. Transactions of Nonferrous Metals Society of China, 2008, 18, 145-149.	4.2	49
186	Synthesis and characteristics of large-scale ZnO rods by wet chemical method. Transactions of Nonferrous Metals Society of China, 2008, 18, 1089-1093.	4.2	10
187	Deposition of electroless Ni-P/Ni-W-P duplex coatings on AZ91D magnesium alloy. Transactions of Nonferrous Metals Society of China, 2008, 18, s323-s328.	4.2	37
188	Enhanced tensile ductility in an electrodeposited nanocrystalline copper. Journal of Materials Research, 2008, 23, 2238-2244.	2.6	20
189	Mechanical behavior of an electrodeposited nanostructured Cu with a mixture of nanocrystalline grains and nanoscale growth twins in submicrometer grains. Journal of Applied Physics, 2008, 104, 084305.	2.5	18
190	Re-examination of Casimir limit for phonon traveling in semiconductor nanostructures. Applied Physics Letters, 2008, 92, 113101.	3.3	24
191	Deformation mechanism transition caused by strain rate in a pulse electric brush-plated nanocrystalline Cu. Journal of Applied Physics, 2008, 104, .	2.5	33
192	Effect of zinc–phosphate–molybdate conversion precoating on performance of cathode epoxy electrocoat on AZ91D alloy. Surface Engineering, 2007, 23, 56-61.	2.2	10
193	Experimental and modelling investigations on strain rate sensitivity of an electrodeposited 20 nm grain sized Ni. Journal Physics D: Applied Physics, 2007, 40, 7440-7446.	2.8	110
194	Effect of substrate temperature on structural properties and photocatalytic activity of TiO2 thin films. Transactions of Nonferrous Metals Society of China, 2007, 17, 772-776.	4.2	22
195	Adsorption of CO on Surfaces of 4d and 5d Elements in Group VIII. Journal of Physical Chemistry C, 2007, 111, 1005-1009.	3.1	55
196	Theoretical Study of C <sub>2</sub> H <sub>2</sub> Adsorbed on Low-Index Cu Surfaces. Journal of Physical Chemistry C, 2007, 111, 18189-18194.	3.1	39
197	Glass Transition of Low-Density Amorphous Water and Related Structures. Journal of Physical Chemistry B, 2007, 111, 11177-11180.	2.6	4
198	Electroless Ni–P layer with a chromium-free pretreatment on AZ91D magnesium alloy. Surface and Coatings Technology, 2007, 201, 4594-4600.	4.8	90

#	Article	IF	CITATIONS
199	Electroless deposition of Ni–W–P coating on AZ91D magnesium alloy. Applied Surface Science, 2007, 253, 5116-5121.	6.1	80
200	Electrochemical synthesis and optical properties of ZnO thin film on In2O3:Sn (ITO)-coated glass. Applied Surface Science, 2007, 253, 7011-7015.	6.1	36
201	Electronic structures and hydrogen bond network of ambient water and amorphous ices. Chemical Physics Letters, 2007, 437, 45-49.	2.6	9
202	Ductile–brittle–ductile transition in an electrodeposited 13 nanometer grain sized Ni–8.6wt.% Co alloy. Materials Science & Engineering A: Structural Materials: Properties, Microstructure and Processing, 2007, 459, 75-81.	5.6	36
203	Micro processing on Cr films by Nd:YAG pulsed laser oxidation method. Journal of Materials Processing Technology, 2007, 184, 173-176.	6.3	6
204	Layered nanostructured Ni with modulated hardness fabricated by surfactant-assistant electrodeposition. Scripta Materialia, 2007, 57, 233-236.	5.2	40
205	Optical and electrical properties of aluminum-doped ZnO thin films grown by pulsed laser deposition. Applied Surface Science, 2007, 253, 3727-3730.	6.1	156
206	Influence of sodium metanitrobenzene sulphonate on structures and surface morphologies of phosphate coating on AZ91D. Transactions of Nonferrous Metals Society of China, 2006, 16, 567-571.	4.2	28
207	Structural and optical properties of nanostructured ZnO thin films deposited on quartz glass. , 2006, , .		1
208	Selected crystallization of water as a function of size. Chemical Physics Letters, 2006, 421, 251-255.	2.6	23
209	Structural and optical properties of ZnO thin films deposited on quartz glass by pulsed laser deposition. Applied Surface Science, 2006, 252, 8451-8455.	6.1	91
210	IR and XPS investigation of visible-light photocatalysis—Nitrogen–carbon-doped TiO 2 film. Applied Surface Science, 2006, 253, 1988-1994.	6.1	170
211	A study and application of zinc phosphate coating on AZ91D magnesium alloy. Surface and Coatings Technology, 2006, 200, 3021-3026.	4.8	152
212	High corrosion-resistance nanocrystalline Ni coating on AZ91D magnesium alloy. Surface and Coatings Technology, 2006, 200, 5413-5418.	4.8	187
213	Electroless Ni–P deposition plus zinc phosphate coating on AZ91D magnesium alloy. Surface and Coatings Technology, 2006, 200, 5956-5962.	4.8	109
214	Growth of zinc phosphate coatings on AZ91D magnesium alloy. Surface and Coatings Technology, 2006, 201, 1814-1820.	4.8	139
215	Al-doped ZnO films by pulsed laser deposition at room temperature. Vacuum, 2006, 81, 18-21.	3.5	51
216	Size and pressure effects on glass transition temperature of poly (methyl methacrylate) thin films. Thin Solid Films, 2006, 497, 333-337.	1.8	11

#	Article	IF	CITATIONS
217	Enhanced tensile ductility in an electrodeposited nanocrystalline Ni. Scripta Materialia, 2006, 54, 579-584.	5.2	113
218	High Strength Nanocrystalline Ni-Co Alloy with Enhanced Tensile Ductility. Advanced Engineering Materials, 2006, 8, 252-256.	3.5	51
219	Strain rate sensitivity of a nanocrystalline Cu synthesized by electric brush plating. Applied Physics Letters, 2006, 88, 143115.	3.3	83
220	Strain rate sensitivity of face-centered-cubic nanocrystalline materials based on dislocation deformation. Journal of Applied Physics, 2006, 99, 076103.	2.5	61
221	AN INVESTIGATION OF SMOOTH NANOSIZED COPPER FILMS ON GLASS SUBSTRATE BY IMPROVED ELECTROLESS PLATING. Surface Review and Letters, 2006, 13, 471-478.	1.1	4
222	A Zinc and Manganese Phosphate Coating on Automobile Iron Castings. ISIJ International, 2005, 45, 1326-1330.	1.4	13
223	Microstructure and photoluminescence properties of ZnO thin films grown by PLD on Si(111) substrates. Applied Surface Science, 2005, 239, 176-181.	6.1	259
224	Single violet luminescence emitted from ZnO films obtained by oxidation of Zn film on quartz glass. Applied Surface Science, 2005, 252, 420-424.	6.1	119
225	ZnO thin film formation on Si(111) by laser ablation of Zn target in oxygen atmosphere. Journal of Crystal Growth, 2005, 279, 447-453.	1.5	35
226	Investigation of nanocrystalline zinc–nickel alloy coatings in an alkaline zincate bath. Surface and Coatings Technology, 2005, 191, 59-67.	4.8	58
227	High corrosion-resistant Ni–P/Ni/Ni–P multilayer coatings on steel. Surface and Coatings Technology, 2005, 197, 61-67.	4.8	97
228	An analytical model for elastic stress field distribution in fibre composite with partially debonded interface. Composites Science and Technology, 2005, 65, 1176-1194.	7.8	17
229	Multilayer Ni-P Coating for Improving the Corrosion Resistance of AZ91D Magnesium Alloy. Advanced Engineering Materials, 2005, 7, 1032-1036.	3.5	36
230	Surface oxidation kinetics of Cr film by Nd-YAG laser. Materials Science & Engineering A: Structural Materials: Properties, Microstructure and Processing, 2005, 391, 210-220.	5.6	10
231	Cr2O3 Film Formed by Surface Oxidation of Stainless Steel Irradiated by a Nd-YAG Pulsed Laser. ISIJ International, 2005, 45, 730-735.	1.4	9
232	Electronic Structures and Hydrogen Bond Network of High-Density and Very High-Density Amorphous Ices. Journal of Physical Chemistry B, 2005, 109, 19893-19896.	2.6	16
233	Electroless Ni–P plating on AZ91D magnesium alloy from a sulfate solution. Journal of Alloys and Compounds, 2005, 391, 104-109.	5.5	127
234	A black phosphate coating for C1008 steel. Surface and Coatings Technology, 2004, 176, 215-221.	4.8	102

#	Article	IF	CITATIONS
235	A new analytical model for three-dimensional elastic stress field distribution in short fibre composite. Materials Science & Engineering A: Structural Materials: Properties, Microstructure and Processing, 2004, 366, 381-396.	5.6	31
236	Dependence of initial stress–strain behavior on matrix plastic inhomogeneity in short fiber-reinforced metal matrix composite. Materials Science & Engineering A: Structural Materials: Properties, Microstructure and Processing, 2004, 369, 93-100.	5.6	2
237	Nano-structured films formed on the AISI 329 stainless steel by Nd-YAG pulsed laser irradiation. Applied Surface Science, 2004, 229, 2-8.	6.1	24
238	Elastic–plastic stress transfer in short fibre-reinforced metal–matrix composites. Composites Science and Technology, 2004, 64, 1661-1670.	7.8	17
239	Synthesis of nanocrystalline NiO/doped CeO2 compound powders through combustion of citrate/nitrate gel. Materials Letters, 2004, 58, 1183-1188.	2.6	14
240	The irradiation effect of a Nd–YAG pulsed laser on the CeO2 target in the liquid. Materials Letters, 2004, 58, 337-341.	2.6	11
241	Synthesis of YSZ nanocrystalline particles via the nitrate–citrate combustion route using diester phosphate (PE) as dispersant. Materials Letters, 2003, 57, 2792-2797.	2.6	34
242	Surface morphology study on chromium oxide growth on Cr films by Nd-YAG laser oxidation process. Applied Surface Science, 2002, 202, 114-119.	6.1	9
243	Stress–strain behavior in initial yield stage of short fiber reinforced metal matrix composite. Composites Science and Technology, 2002, 62, 841-850.	7.8	18
244	An analytical study of the influence of thermal residual stresses on the elastic and yield behaviors of short fiber-reinforced metal matrix composites. Materials Science & Engineering A: Structural Materials: Properties, Microstructure and Processing, 1998, 248, 256-275.	5.6	56
245	Effects of microstructural variables on the deformation behaviour of dual-phase steel. Materials Science & Engineering A: Structural Materials: Properties, Microstructure and Processing, 1995, 190, 55-64.	5.6	150
246	A composite model for superplasticity. Journal of Materials Science, 1995, 30, 1977-1981.	3.7	6
247	A dislocation density approximation for the flow stress—grain size relation of polycrystals. Acta Metallurgica Et Materialia, 1995, 43, 3349-3360.	1.8	41
248	On the enhanced grain growth in ultrafine grained metals. Acta Metallurgica Et Materialia, 1995, 43, 4165-4170.	1.8	138
249	Numerical analysis of the influence of various factors on forming the limit of hydrostatic bulging for ductile materials. Computers and Structures, 1994, 50, 677-684.	4.4	4
250	Deformation behaviour of ultra-fine-grained copper. Acta Metallurgica Et Materialia, 1994, 42, 2467-2475.	1.8	547
251	Model for the prediction of the mechanical behaviour of nanocrystalline materials. Materials Science & Engineering A: Structural Materials: Properties, Microstructure and Processing, 1993, 172, 23-29.	5.6	101
252	The relationship between ductility and material parameters for dual-phase steel. Journal of Materials Science, 1993, 28, 1814-1818.	3.7	38

#	Article	IF	CITATIONS
253	A modified Hall-Petch relationship for nanocrystalline materials. Scripta Materialia, 1993, 2, 415-419.	0.5	40
254	A new relationship between the flow stress and the microstructural parameters for dual phase steel. Acta Metallurgica Et Materialia, 1992, 40, 1587-1597.	1.8	31
255	Finite-element numerical analysis of sheet metal under uniaxial tension with a new yield criterion. Journal of Materials Processing Technology, 1992, 31, 245-253.	6.3	4
256	Isotropic polycrystal yield surfaces of b.c.c. and f.c.c. metals: crystallographic and continuum mechanics approaches. Acta Metallurgica Et Materialia, 1991, 39, 2285-2294.	1.8	14
257	Influence of predeformation on microstructure and mechanical properties of 1020 dual phase steel. Materials Science and Technology, 1991, 7, 527-532.	1.6	13
258	Plastic instability and strain to fracture for damaged materials. Materials Science & Engineering A: Structural Materials: Properties, Microstructure and Processing, 1991, 131, 9-15.	5.6	8
259	Theoretical model for the tensile work hardening behaviour of dual-phase steel. Materials Science & Engineering A: Structural Materials: Properties, Microstructure and Processing, 1991, 147, 55-65.	5.6	75
260	Plastic behavior and stretchability of sheet metals. Part I: A yield function for orthotropic sheets under plane stress conditions. International Journal of Plasticity, 1989, 5, 51-66.	8.8	1,040
261	Plastic behaviour and stretchability of sheet metals. Part II: Effect of yield surface shape on sheet forming limit. International Journal of Plasticity, 1989, 5, 131-147.	8.8	119
262	Diffuse necking and localized necking under plane stress. Materials Science & Engineering A: Structural Materials: Properties, Microstructure and Processing, 1989, 111, 1-7.	5.6	13
263	Application of Hill's new yield theory to sheet metal forming—Part I. Hill's 1979 criterion and its application to predicting sheet forming limit. International Journal of Mechanical Sciences, 1989, 31, 237-247.	6.7	40
264	Application of Hill's new yield theory to sheet metal forming—Part II. A numerical study of hydrostatic bulging using Hill's 1979 yield criterion. International Journal of Mechanical Sciences, 1989, 31, 249-263.	6.7	9
265	Influence of variation of strain rate sensitivity on limit strain of superplasticity. Scripta Metallurgica, 1987, 21, 331-334.	1.2	5
266	Forming limit diagram of sheet metal in the negative minor strain region. Materials Science and Engineering, 1987, 86, 137-144.	0.1	40
267	Numerical analysis of superplastic bulging for cavity-sensitive materials. International Journal of Mechanical Sciences, 1987, 29, 565-576.	6.7	19
268	Numerical Analysis of the Influence of Various Defects on Superplastic Fracture Under Uniaxial Tension. Studies in Applied Mechanics, 1987, 15, 213-220.	0.4	1
269	Necking development and strain to fracture under uniaxial tension. Materials Science and Engineering, 1986, 84, 157-162.	0.1	30
270	Enhanced tensile ductility in an electrodeposited nanocrystalline Ni. , 0, , .		1